SSRG International Journal of Mechanical Engineering
ISSN: 2348-8360/ https://doi.org/10.14445/23488360/IJME-V13I3P104

Volume 13 Issue 3, 44-53, March 2026

Original Article

Finite Volume Method for Coupled Hydrodynamic Sediment Transport Model with Adaptive Mesh Refinement

Mohammed Frihessane[1*], Ouafae Boulerhcha[1], Salah Daoudi[1]

[1]*Département de Physique, UMP, Oujda, Morocco.*

**Corresponding Author : mohammed.frihesssane.ump.ac.ma*

Received: 20 December 2025 Revised: 22 January 2026 Accepted: 20 February 2026 Published: 28 March 2026

Abstract *- A river flow with sediments of different sizes shows two modes of transport. Fine particles move in suspension, while coarse grains are transported as bedload. The process is governed by the Saint Venant equations for water flow, the advection-diffusion equation for suspended sediments, and the Exner equation for bedload. In our model, erosion and deposition are handled separately. The net sediment flux is found from the difference between the eroded and deposited masses. The full system is a set of nonlinear partial differential equations. It is solved with the finite volume method on unstructured meshes, using a second-order SRNH scheme in time and space. To make the computation more efficient, we use adaptive mesh refinement to add resolution where sediment concentration changes fast. The method is tested on several cases that combine flow and sediment transport, such as dam-break problems.*

Keywords *- Sediment transport, Coupled model, Shallow water.*

1. Introduction

Water flow is the primary cause of sediment transport; it erodes the riverbed in some places and deposits the transported materials in other places. These changes to the riverbed alter the river's topography, which in turn changes the flow characteristics [1, 2]. Understanding the phenomenon of sediment transport is therefore essential for predicting the morphological evolution of rivers and for planning the management of infrastructure subject to erosion and sedimentation. Erosion and sedimentation processes are generally described by empirical laws that depend on flow characteristics and bed morphology. These features vary considerably over time and space, making bed and flow evolution particularly difficult [3].

In this study, two sediment transport modes are examined: (i) suspension transport and (ii) bedload transport [4, 5]. The former involves fine particles that are carried in suspension by the flow over long distances. In this regime, the concentration of the water sediment mixture is governed by the hydrodynamic conditions of the flow (e.g., mean velocity and turbulence intensity) as well as by the physical properties of the particles, including size, shape, and density.

By contrast, bedload transport involves the movement of coarser particles that move along the riverbed by: (i) rolling, (ii) sliding, or (iii) saltation under the influence of shear stress exerted by the flowing water. This transport mode is irregular and occurs only when the flow velocity exceeds a critical threshold required to overcome gravitational and resisting forces.

These transport modes control channel bed variability and river morphological evolution. Sediment transport in shallow water flows has been widely studied. Some authors [14] adopt a decoupled approach, solving the hydrodynamic equations first and then the Exner equation, while others employ a fully coupled model. Many studies, such as [4], using the finite volume framework, rely on fixed meshes, which limit their ability to accurately capture shock waves generated during dam-break flows [4-7, 12-14].

This study has the objective of developing a coupled hydrodynamic-sediment transport model based on the finite volume method. This last employs the SRNH (non-homogeneous Riemann solution) scheme, which represents a second-order accurate scheme in both time and space, and is implemented on unstructured meshes with an adaptive mesh refinement strategy. This approach enhances both accuracy and computational efficiency in regions characterized by strong water–sediment concentration gradients. The model is validated through several numerical experiments, including dam-break simulations over erodible beds. The results demonstrate the effectiveness of the proposed model and

highlight its strong potential for practical applications in hydraulic engineering and river management [5, 8].

The plan of this paper is as follows: The 2nd and 3rd sections represent the mathematical model and the numerical scheme. Section 4 is a brief presentation of the adapted mesh procedure. In Section 5, we show in the section 5 the core of the work, which is the validation of the method and its application to post-dam failure flows. Section 6 is a conclusion.

2. Mathematical Model

The mathematical model governing sediment transport is composed of three highly coupled equations:

- Saint-Venant equations: these govern the conservation of mass and momentum of fluid.
- Advection-diffusion equation: this governs the transport of very fine grains in suspension.
- Exner equation: this describes the evolution of the riverbed over time, taking into account erosion and deposition of bottom sediments.
- The model also includes source terms representing friction with the bed and banks, as well as erosion and sediment deposition. The mathematical model is written as:

Where $(x, y)$are the horizontal coordinates, variable t is the time, (u,v) are the velocity components, and h is the water depth. The variable C is the average concentration of the water-sediment mixture, Z_b is the bed elevation, g is the gravitational acceleration. $A_g$is a coefficient belonging to the interval]0,1[, p is the porosity, $\xi = \frac{1}{1-p}$, ϱ=$\varrho_w(1-C)+\varrho_s C$ is the density of the water sediment mixture, $\varrho_0 = \varrho_w p + \varrho_s(1-p)$ is the density of the saturated bed, ϱ_w is water density, ϱ_s is the density of solid particles. $S_f^x$and S_f^y are the frictional stresses defined by Manning's relations:

$$S_f^x = -n^2 \frac{u\sqrt{u^2+v^2}}{h^{4/3}}, \qquad S_f^y = -n^2 \frac{v\sqrt{u^2+v^2}}{h^{4/3}}$$

n is the Manning coefficient.

When the fluid velocity increases, we observe an increase in suspended particles; conversely, when the fluid velocity decreases, we observe an increase in particle deposition. The net balance between particles that settle and those that float will be represented by D and E. The deposition (D) and erosion (E) terms are empirically defined as:

$$D = \left[\sqrt{\left(\frac{13.95\nu}{d}\right)^2 + 1.09\left(\frac{\varrho_s}{\varrho_w}-1\right)gd} - \frac{13.95\nu}{d}\right](1 - \alpha C).\alpha C$$

and

$$E = \begin{cases} \eta(\theta-\theta_c)h^{-1}d^{0.2}\sqrt{u^2+v^2} & \text{if } \theta > \theta_c \\ 0 & \text{otherwise} \end{cases}$$

Where ν is the kinematic viscosity of water, d is the diameter of the grain, α is an empirical coefficient given by $\alpha = min\left(2, \frac{1-p}{c}\right)$ and θ_c is the critical Shields parameter, which has an experimental value of θ_c=0.047, η is a coefficient that controls erosion, and $\theta = \frac{hS_f}{\left(\frac{\varrho_s}{\varrho_w}-1\right)d}$ is the dimensionless shear stress.

The system (1) without source terms is strictly hyperbolic, let

$$A = \left[\frac{\partial F}{\partial x}\right] \text{ and } B = \frac{\partial G}{\partial x}$$

be the Jacobian matrices associated with F and G. For any direction $\mathrm{n} = (n_x, n_y)$, the Jacobian matrix in the direction n is defined as:

$$J = An_x + Bn_y \tag{7}$$

3. Discretization Scheme

3.1. Non-Homogeneous Riemann Solution Scheme (SRNH-Scheme)

The finite volume method consists, in a first step, of partitioning the domain Ω into triangles T_i. This choice offers great flexibility for handling complex geometries or for mesh refinement [5, 6]. Here, we consider a cell-centered formulation, where the mesh triangles coincide with control volumes.

The variational form of the problem (1) is:

$$\int_{T_i}\frac{\partial W}{\partial t}d\Omega + \int_{T_i}\frac{\partial F(W)}{\partial x}d\Omega + \int_{T_i}\frac{\partial G(W)}{\partial y}d\Omega + \int_{T_i}\frac{\partial G(W)}{\partial y}d\Omega = \int_{T_i} S(W)d\Omega + \int_{T_i} Q(W)d\Omega \tag{8}$$

Applying Green's theorem to T_i with area A_i, we obtain:

$$\frac{\partial W_i}{\partial t} + \frac{1}{A_i}\sum_{j=1}^{3}\int_{\Gamma_{ij}}\mathcal{F}(W, n_{ij})d\Gamma = S_i + Q_i \tag{9}$$

- W_i, S_i, Q_i are the average values over the cell T_i
- Γ_{ij} is the interface between T_i and T_j.
- n_{ij}=(n_x, n_y) is the unit normal directed from T_i to T_j.
- $\mathcal{F}(W, n_{ij})$=$F(W).\ n_x + G(W).n_y$

We use the explicit Euler scheme to discretize time:

$$W_i^{n+1} = W_i^n - \frac{\Delta t}{A_i}\sum_{j=1}^{3}\int_{\Gamma_{ij}}\mathcal{F}(W, n_{ij})d\Gamma + \Delta t.S_i^n + \Delta t.Q_i^n \tag{10}$$

We omit the term Q, which will be calculated later by a partitioning procedure [9], then we have:

$$W_i^{n+1} = W_i^n - \frac{\Delta t}{A_i}\sum_{j=1}^{3}\int_{\Gamma_{ij}} \mathcal{F}\left(W, n_{ij}\right)d\Gamma + \Delta t.S_i^n \quad (11)$$

We use the numerical flux $\mathcal{F}\left(W_i, W_j, \mathrm{n}_{ij}\right)$ to calculate convective flux:

$$\int_{\Gamma_{ij}} \mathcal{F}\left(W,\mathrm{n}_{ij}\right)d\Gamma = \mathcal{F}\left(W_i, W_j, \mathrm{n}_{ij}\right)\left|\Gamma_{ij}\right| \quad (12)$$

Where $\left|\Gamma_{\mathrm{ij}}\right|$ is the length of the edge Γ_{ij} .

By construction of the SRNH scheme (Non-Homogeneous Riemann Solver), the numerical flux is given by:

$$\mathcal{F}\left(W_i, W_j,\ \mathrm{n}_{ij}\right)=\mathcal{F}\left(W_{\mathrm{ij}}^{\mathrm{n}},\ \mathrm{n}_{ij}\right)$$

Where $W_{\mathrm{ij}}^{\mathrm{n}}$ is determined in the prediction step by:

$$W_{ij}^n = \frac{1}{2}\left(W_i + W_j\right) - \frac{1}{2}\mathrm{sgn}\left[J\left(\overline{W}_{ij}^{\,n}, \mathrm{n}_{ij}\right)\right]\left(W_j - W_i\right) \quad (13)$$

- $\overline{W}_{ij}^{\,n}$ is the Roe average on the interface Γ_{ij}.
- $J\left(\overline{W}_{ij}^{\,n}, \mathrm{n}_{ij}\right) = \frac{\partial F}{\partial x}n_x + \frac{\partial F}{\partial y}n_y$ is the Jacobian matrix (7) evaluated at the Roe average state W_{ij}^n at time t^n.
- $\mathrm{sgn}\left[J\left(\overline{W}_{ij}^{\,n}, \mathrm{n}_{ij}\right)\right]$ represents the sign matrix of $J\left(\overline{W}_{ij}^{\,n}, \mathrm{n}_{ij}\right)$.

The solution at the time t^{n+1} is then determined in the correction step by:

$$W_i^{n+1} = W_i^n - \frac{\Delta t}{A_i}\sum_{j=1}^{3}\mathrm{F}\left(W_i, W_j, \mathrm{n}_{ij}\right)\left|\Gamma_{ij}\right| + \Delta t.S_i^n \quad (14)$$

For more details on the calculation of the sign matrix and source terms, we refer the reader to references [5, 6].

3.2. Temporal Discretisation

We discretize time using a second-order Runge-Kutta scheme; for this, we use form (9) of our system to be solved:

$$\frac{\partial W}{\partial t} = \mathcal{L}(W)$$

Then we have : $\begin{cases} \overline{W}^{n+1} = W^n + \frac{\Delta t}{2}\mathcal{L}(W^n) \\ W^{n+1} = W^n + \Delta t\mathcal{L}(\overline{W}^{n+1}) \end{cases}$

4. Mesh Adaptation

The choice of mesh density will influence both the computational cost and the quality of the numerical solution. Capturing the solution in shock zones requires a very fine grid. However, in complex flows, the regions where these shocks occur are not known a priori. It is therefore not possible to construct an optimal mesh from the start, i.e., a mesh capable of accurately capturing shocks with a minimal number of elements. The best strategy is then to adapt the mesh during the computation, either by enriching it or by optimally re-meshing it as the solution evolves.

The algorithm used here relies on a multi-level data structure. It dynamically remeshes the computational domain as the solution evolves. In practice, the solution is calculated on a coarse mesh, areas where the gradients of the variable chosen as the refinement criterion (here, concentration) are strong are identified, and these are subdivided into four triangles. Conversely, cells where the solution is smooth are derefined [3, 5].

The coarse mesh elements are called “triangles of level 0 “, while their sons are “triangles of level 1”, and so on (figure 1).

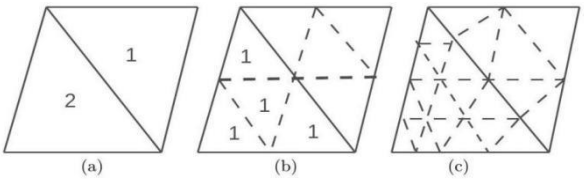

Fig. 1 Refinement: (a) Level 0, (b) Level 1, (c) Level 2.

5. Numerical Validation

5.1. C-Property: Study Flow Over a Hump

On the square domain [0,100]×[0,100] we consider hump of equation [11] :

$$Z(x,y) = 0.8\exp\left(-50\left(\frac{x}{100} - 0.5\right)^2 - -50\left(\frac{y}{100} - 0.5\right)^2\right)$$

Initially, the water height is given by:

$$h = 2 - Z(x,y)$$

and the fluid is at rest. On the boundaries, we impose the Neumann conditions.

We use two types of mesh: the first is structured and contains 8281 nodes and 16200 elements; the second is unstructured and contains 800 nodes and 1502 elements. We stop the calculations at t = 200 s.

The error, defined by $\varepsilon = \left||Z + \mathrm{h} - 2|\right|$, is $\varepsilon = 0.7958\ 10^{-16}$ on the first mesh and $\varepsilon = 0.8499\ 10^{-16}$ on the second mesh. So, despite the variation of the bed elevation, the free surface remains horizontal; we can therefore certify that the scheme verifies the C-property.

5.2. Dam Break Over Mobile Bed

The first application concerns the flow after a dam break in a rectangular channel with a flat bottom. The channel is 50,000 m long and 1,000 m wide; the sediments are assumed to be non-cohesive with a diameter d = 8 mm. The

computational mesh is structured and comprises 10,521 nodes and 20,000 elements (Figure 2). We start with the following initial conditions:

$$\begin{cases} h(x,y) = \begin{cases} 40\ m \text{ if } x \leq 25{,}000\ m \\ 2\ m \text{ if } x > 25{,}000\ m \end{cases} \\ u(x,y) = 0\ m/s;\ \ C(x,y) = 0.001 \end{cases}$$

Our objective with this test is to compare the SRNH scheme with the modified-Roe scheme described in reference [8]. Figures 3 and 4 show, at times t=5, 10, 15, and 20 min, the free surface profiles. Figures 5 and 6 show profiles of concentration at the same times. All these figures are obtained along the y=500 cross-section. Very good agreement is observed between the two approaches, confirming the reliability of the proposed method.

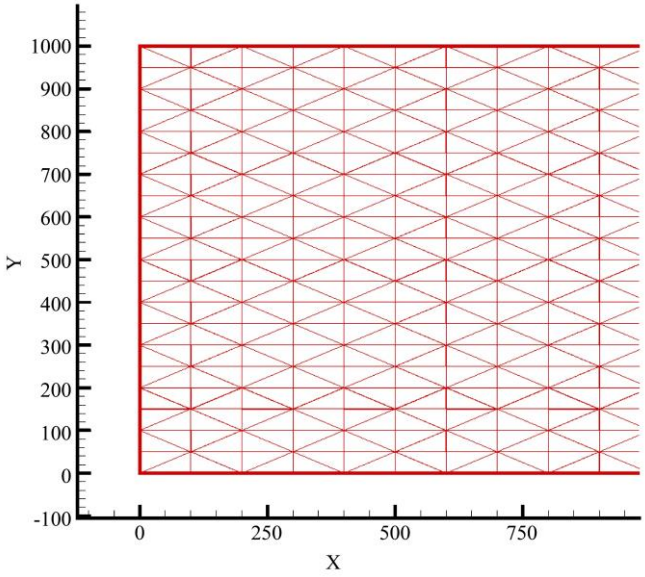

Fig. 2 Structured mesh

5.3. Partial Dam Break Over Erodable Bed

The computational domain is a square reservoir measuring 200 m x 200 m with a flat bed. Initially, a dam of thickness 4 m is located at x=100 m. This dam contains a breach of 75 m long (Figure 7). The sediments are assumed to be non-cohesive with a diameter of 2 mm.

We start the calculations on a structured mesh containing 2,601 nodes and 4,938 elements (Figure 8). However, the computations are performed on an unstructured mesh that evolves dynamically through a regular refinement/derefinement procedure.

The initial conditions are:

$$\begin{cases} Z(x,y) = 0 \\ u(x,y) = v(x,y) = 0 \\ h(x,y) = \begin{cases} 10, & \text{if } x \leq 100 \\ 1, & \text{if } x > 100 \end{cases} \\ C(x,y) = \begin{cases} 0.01, & \text{if } x \leq 100 \\ 0, & \text{if } x > 100 \end{cases} \end{cases}$$

Figure 9 shows the dynamic meshes obtained by applying the mesh refinement/derefinement procedure at times t = 2, 4, 6, 8 s. Figure 10 shows the bed shape isovalues at the same times.

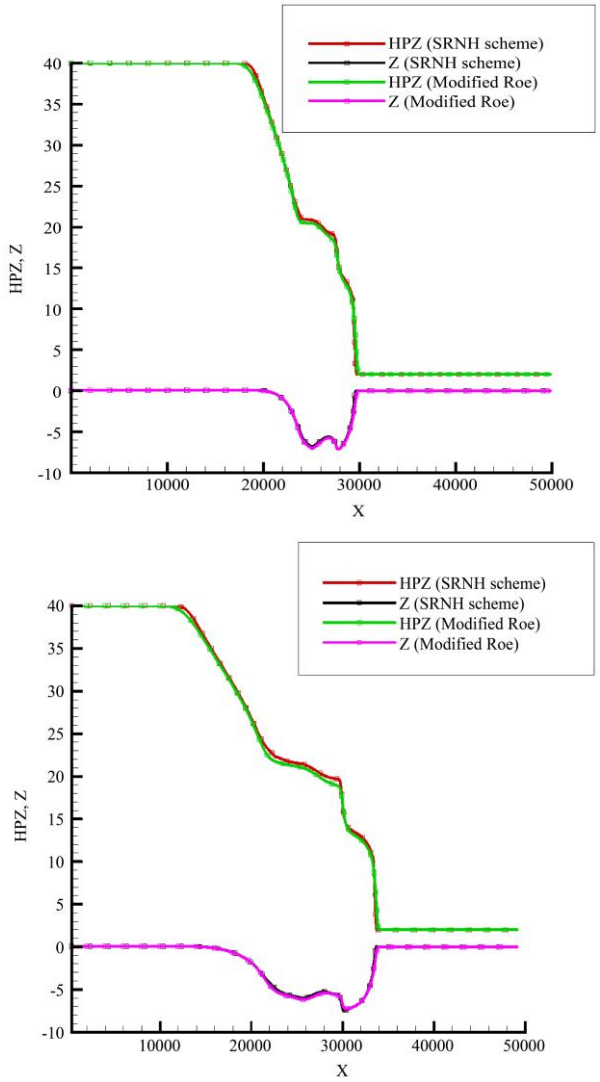

Fig. 3 Evolution of free surface and bed erosion at times t=5, 10 min

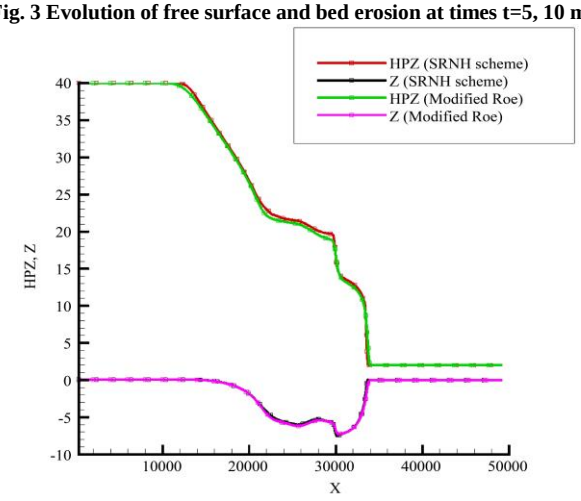

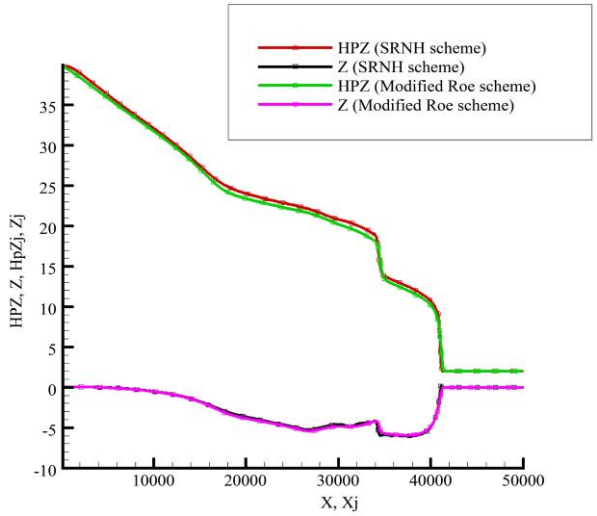

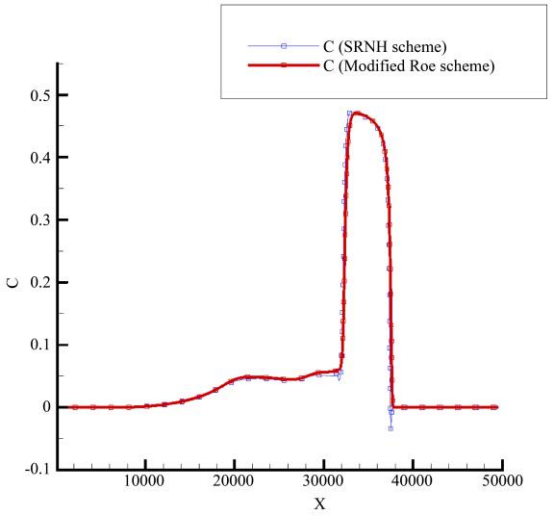

Fig. 4 Evolution of free surface and bed erosion at times t=15, 20 min

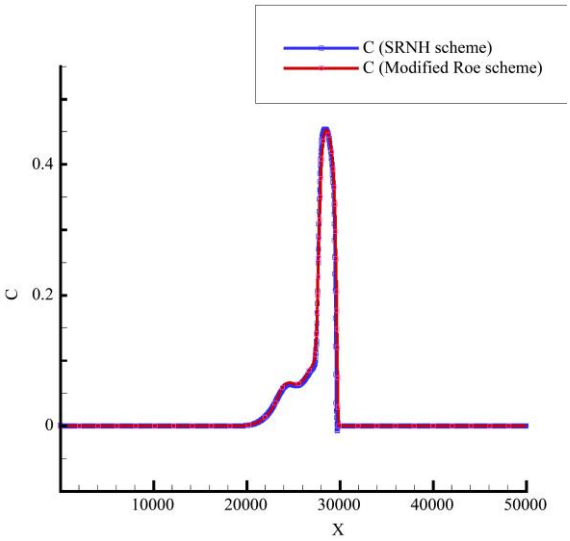

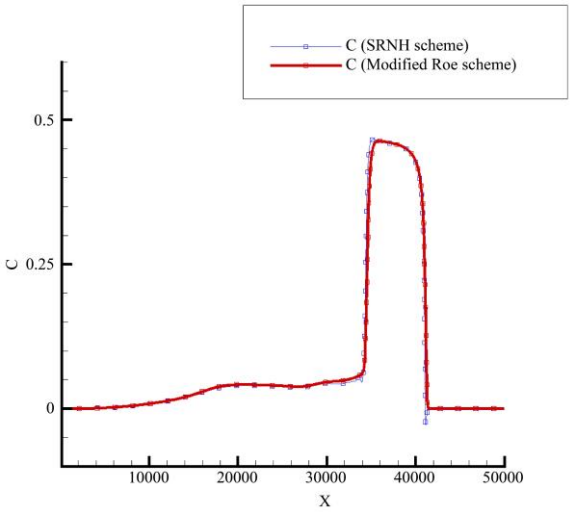

Fig. 6 Evolution of concentration at times t=15, 20 min

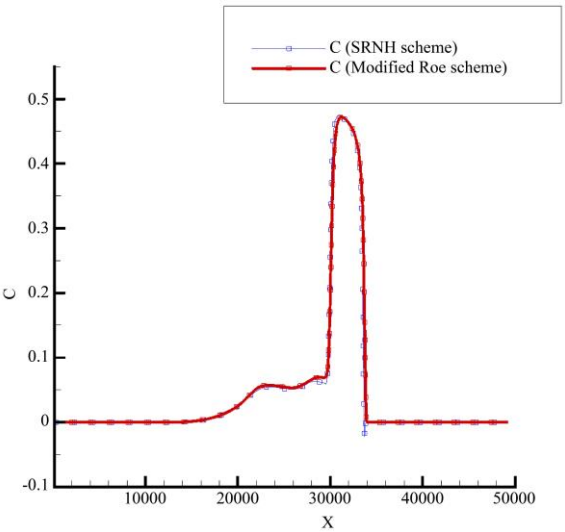

Fig. 5 Evolution of concentration at times t=5, 10 min

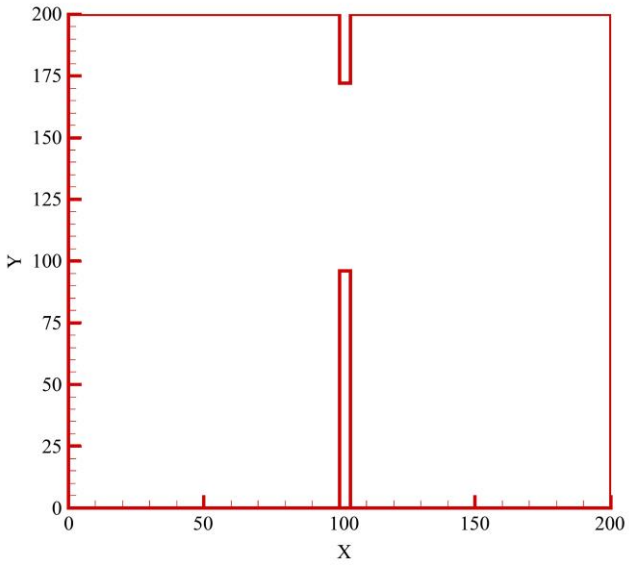

Fig. 7 Computational domain

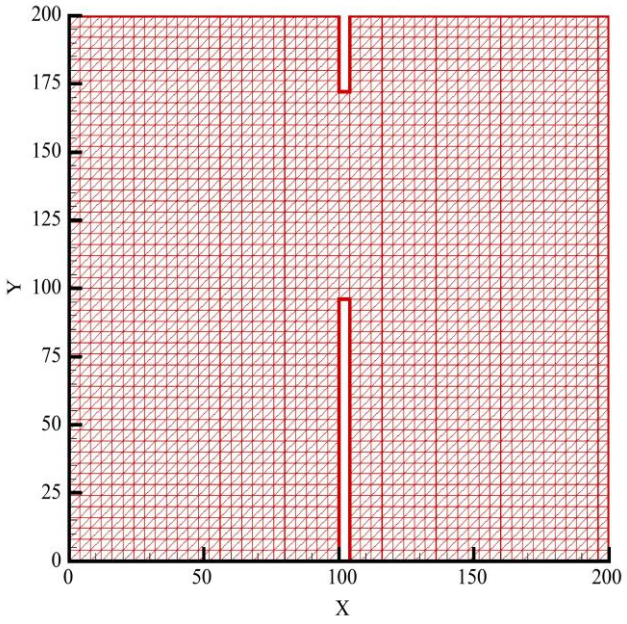

Fig. 8 Initial mesh

Figures 11 and 12 present the free surface and concentration isovalues at the same times. Figures 13 and 14 show the values of the free surface, bed shape, and concentration along the y = 125 section at times t = 2, 4, 6, 8 s for the particle with a diameter of 2 mm.

Firstly, we compared our results obtained by the SRNH scheme with those reported in reference [8] obtained by the Modified-Roe scheme, and we can certify that they are in very good agreement.

We note that the choice of concentration gradient as an indicator of refinement proves to be excellent; we observe that the mesh is very dense in the vicinity of the upstream and downstream wave fronts and that it follows the movement of these wave fronts well (Figure 9).

As expected, grain size has a significant influence on the free surface profile. In the presence of fine particles, we observe the appearance of a pronounced hydraulic jump, resulting in an abrupt transition in the flow regime. In contrast, for larger sediments, the transition is less abrupt.

Furthermore, the extent of bed erosion depends strongly on the size of the sediments. When sediment particles are fine, erosion is greater: a larger quantity of bed material is easily suspended and incorporated into the water-sediment mixture.

Conversely, for coarser sediments, erosion is considerably lower. This behavior is expected and straightforward, as smaller particles are transported effortlessly by the flow due to their lower settling velocity and reduced resistance to shear forces.

As for the concentrations and as illustrated in Figure 14, one can clearly observe that the finest sediments correspond to higher concentration values.

This is mainly observed for the concentration curve related to d=2mm and d = 8 mm at t = 8 sec. Besides, the wavefront undergoes lateral expansion, as shown by the concentration profiles at t = 8 sec. This expansion is more pronounced for the finer sediments, which remain in suspension longer.

This can be physically explained by the fact that fine particles have a lower sedimentation rate and tend to disperse more easily, while coarse particles settle more quickly under comparable hydraulic conditions.

6. Conclusion

The objective of this study is the development of an efficient numerical approach for modeling sediment transport, including both suspension and bedload methods. The used mathematical model couples the Saint Venant equations together with the convection-diffusion equation and the Exner equation.

The numerical implementation is based on the finite volume method using the SRNH scheme, which employs a second-order Runge-Kutta technique for time integration and the Minmod limiter to achieve second-order accuracy in space.

It has been observed that the implementation of an adaptive mesh refinement strategy based on concentration gradients improves the computational efficiency while enhancing wavefront resolution.

The used method was validated through several tests, including verification of the C-property, dam break simulations, and partial dam failure scenarios, showing excellent agreement with the already published results in the literature.

Another important aspect that has been addressed is the influence of sediment grain size on bed evolution and water-sediment mixture concentration. Results highlight that finer grains result in greater erosion and higher transport in suspension.

Besides, coupling the second-order SRNH scheme with adaptive mesh refinement yields a stable, efficient, and accurate approach (in comparison to the literature), highlighting the model's strong potential for hydraulic engineering and river management applications.

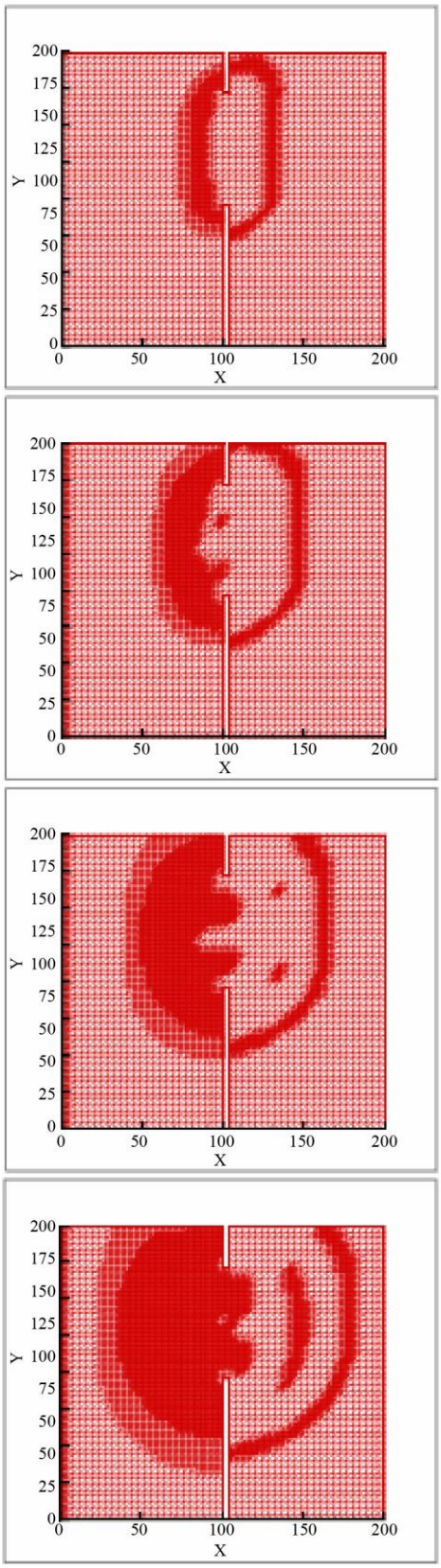

Fig. 9 Dynamic meshes at times t = 2, 4, 6, 8 s

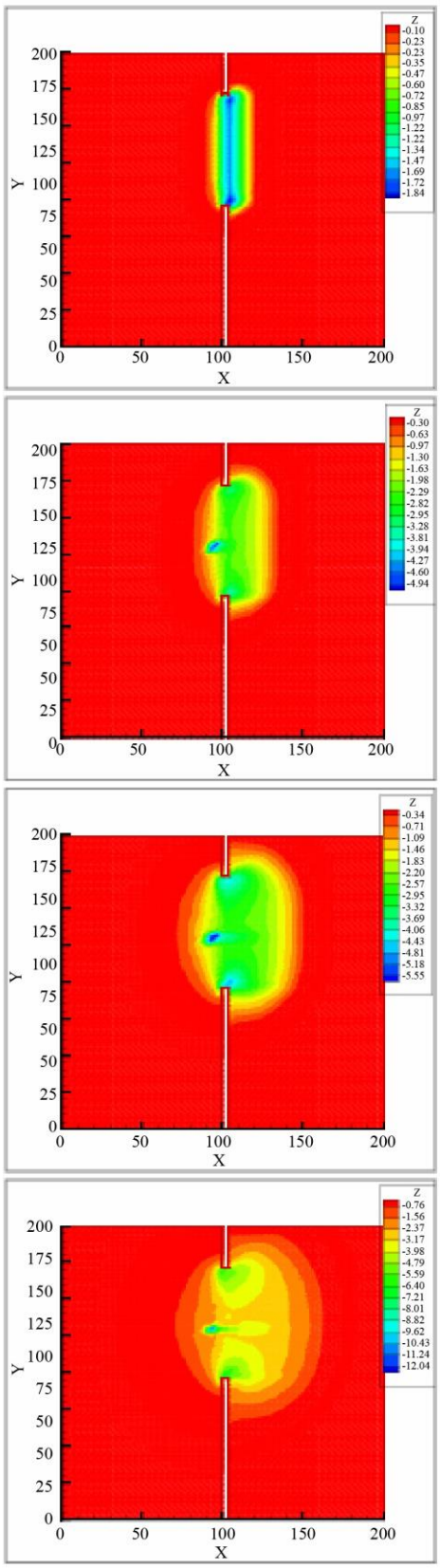

Fig. 10 Bed shape isovalues at times t = 2, 4, 6, 8 s

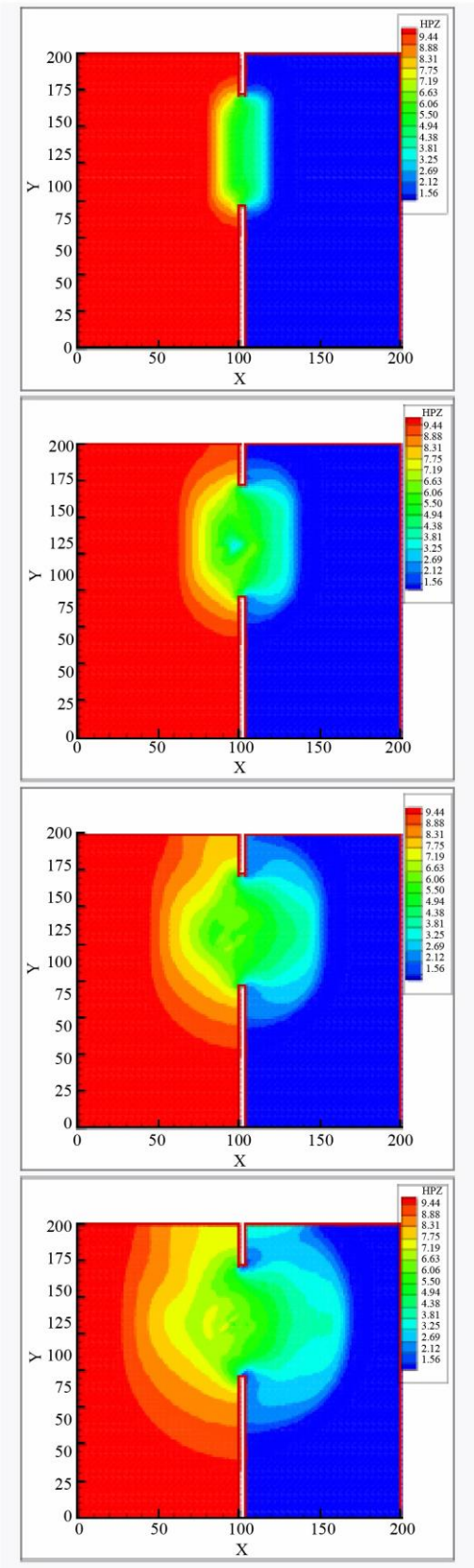

Fig. 11 Free surface isovalues at times t = 2, 4, 6, 8 s

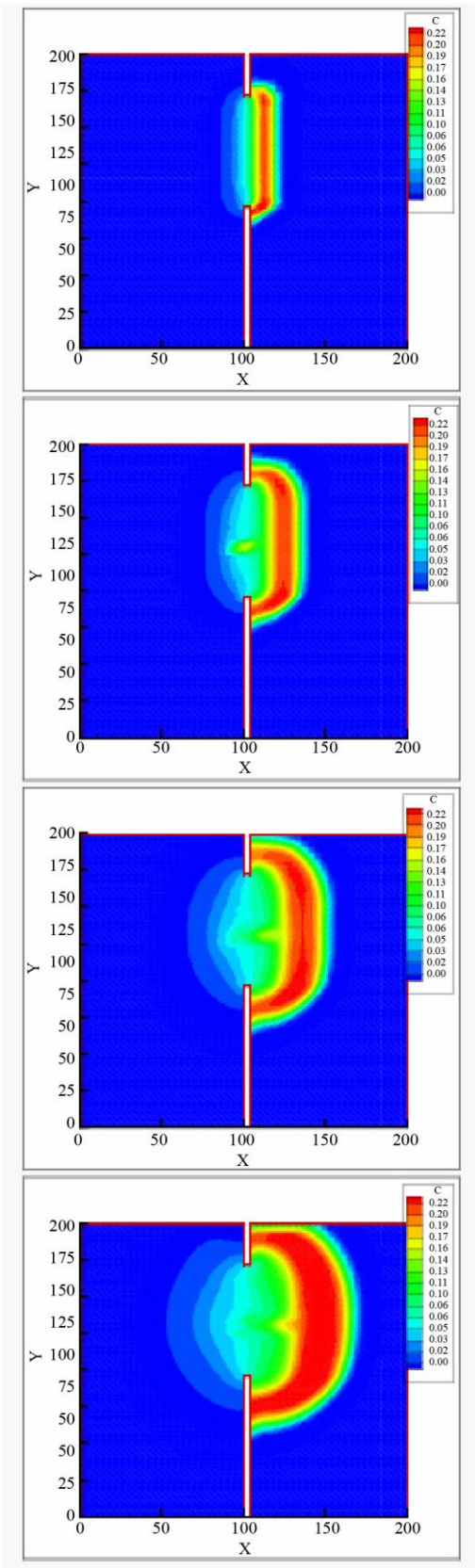

Fig. 12 Concentration isovalues for at times t = 2, 4, 6, 8 s

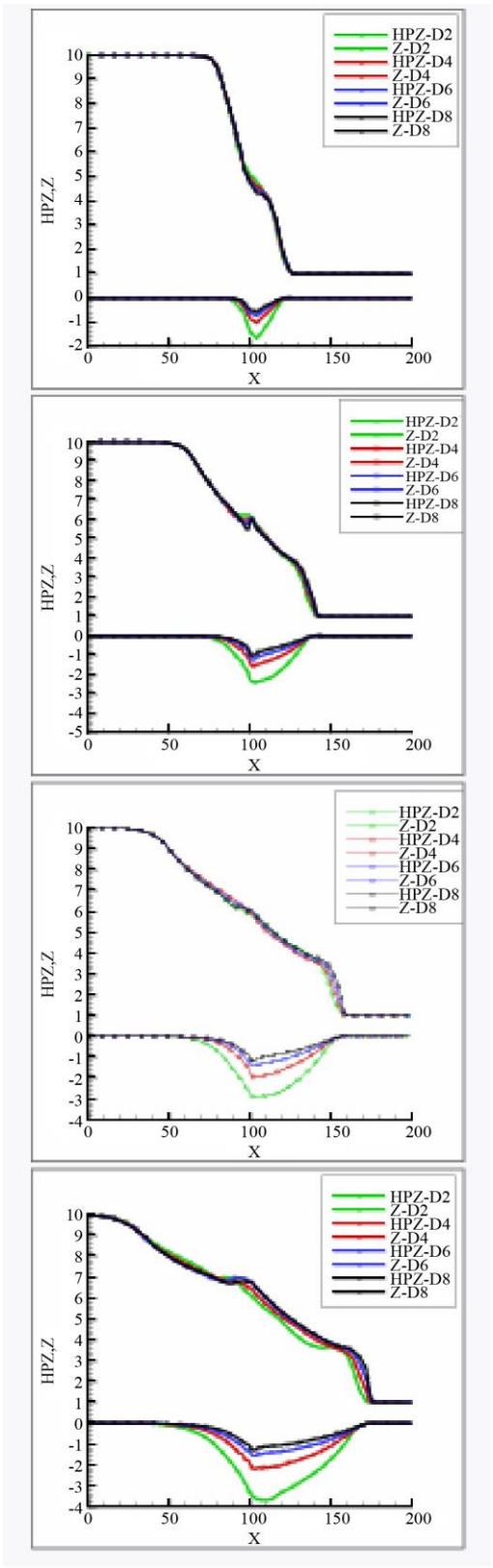

Fig. 13 Free surface and bed erosion at times t = 2, 4, 6, 8 s

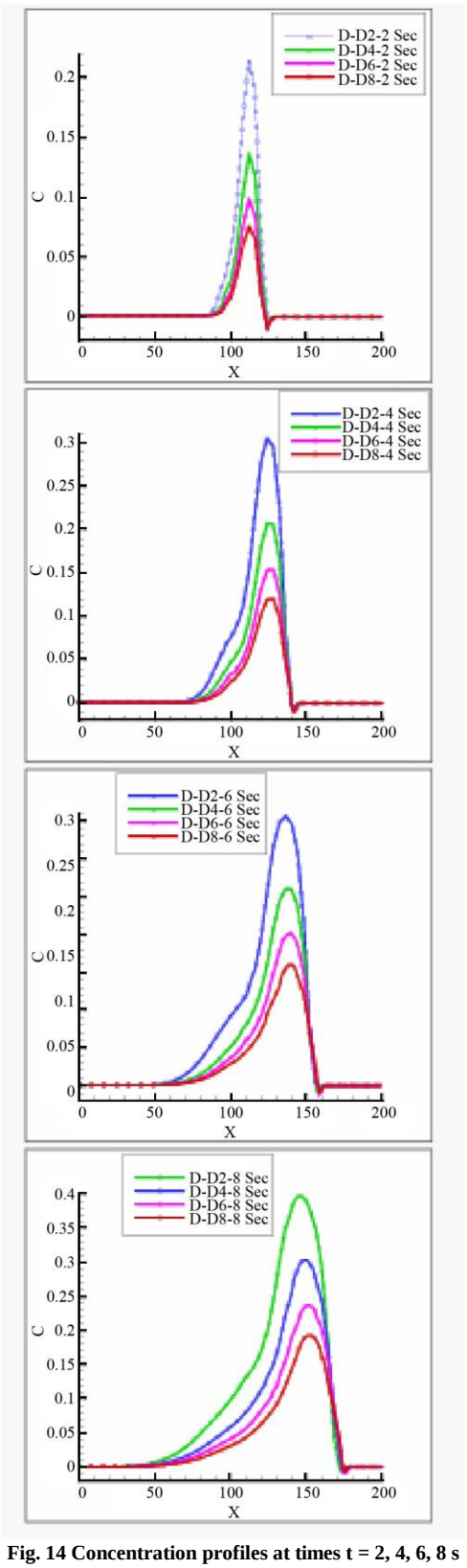

Fig. 14 Concentration profiles at times t = 2, 4, 6, 8 s

References

[1] Fabien Souillé, Nicolas Claude, and Magali Jodeau, "A Numerical Model for Simulation of Bedload Transport in Unsteady Trans-Critical River Flow," *Environmental Modelling and Software*, vol. 192, 2025. [CrossRef] [Google Scholar] [Publisher Link]

[2] Weiming Wu, *Computational River Dynamics*, Taylor & Francis, pp. 1-494, 2008. [Google Scholar] [Publisher Link]

[3] Jia-heng Zhao et al., "Comparison of Depth-Averaged Concentration and Bed Load Flux Sediment Transport Models of Dam-Break Flow," *Water Science and Engineering*, vol. 10, no. 4, pp. 287-294, 2017. [CrossRef] [Google Scholar] [Publisher Link]

[4] Xin Liu, and Abdelaziz Beljadid, "A Coupled Numerical Model for Water Flow, Sediment Transport and Bed Erosion," *Computers and Fluids*, vol. 154, pp. 273-284, 2017. [CrossRef] [Google Scholar] [Publisher Link]

[5] Fayssal Benkhaldoun et al., "An Unstructured Finite Volume Method for Coupled Models of Suspended Sediment and Bed Load Transport in Shallow-Water Flows," *International Journal for Numerical Methods in Fluids*, vol. 72, no. 9, pp. 967-993, 2013. [CrossRef] [Google Scholar] [Publisher Link]

[6] Fayssal Benkhaldoun, Imad Elmahi, and Mohammed Seaïd, "A New Finite Volume Method for Flux ‐ Gradient and Source ‐ Term Balancing in Shallow Water Equations," *Computer Methods in Applied Mechanics and Engineering*, vol. 199, no. 42-52, pp. 3324-3335, 2010. [CrossRef] [Google Scholar] [Publisher Link]

[7] Sanae Jelti, M. Mezouari, and M. Boulerhcha, "Numerical Modeling of Dam-Break Flow Over Erodible Bed by Roe Scheme with an Original Discretization of Source Term," *International Journal of Fluid Mechanics Research*, vol. 45, no. 1, pp. 21-36, 2018. [CrossRef] [Google Scholar] [Publisher Link]

[8] S. Jelti, and M. Boulerhcha, "Numerical Modeling of Two-Dimensional Noncapacity Model for Sediment Transport by an Unstructured Finite Volume Method with a New Discretization of the Source Term," *Mathematics and Computers in Simulation*, vol. 197, pp. 253-276, 2022. [CrossRef] [Google Scholar] [Publisher Link]

[9] S.J. Billet, and E.F. Toro, "On WAF-Type Schemes for Multidimensional Hyperbolic Conservation Laws," *Journal of Computational Physics*, vol. 130, no. 1, pp. 1-24, 1997. [CrossRef] [Google Scholar] [Publisher Link]

[10] ZhiYuan Yue et al., "Two-Dimensional Coupled Mathematical Modeling of Fluvial Processes with Intense Sediment Transport and Rapid Bed Evolution," *Science in China Series G: Physics, Mechanics and Astronomy*, vol. 51, pp. 1427-1438, 2008. [CrossRef] [Google Scholar] [Publisher Link]

[11] M. Mezouari et al., "Transport of Pollutants in the Nador Lagoon (Morocco) by the Finite Volume Method with SRNH Scheme," *Physical and Chemical News*, vol. 63, pp. 61-72. 2025. [Publisher Link]

[12] Zhixian Cao et al., "Computational Dam-Break Hydraulics Over Erodible Sediment Bed," *Journal of Hydraulic Engineering*, vol. 130, no. 7, pp. 389-703, 2004. [CrossRef] [Google Scholar] [Publisher Link]

[13] Chaojun Ouyang, Siming He, and Qiang Xu, "MacCormack-TVD Finite Difference Solution for Dam-Break Hydraulics Over Erodible Sediment Beds," *Journal of Hydraulic Engineering*, vol. 141, no. 5, pp. 1-9, 2014. [CrossRef] [Google Scholar] [Publisher Link]

[14] Luigi Fraccarollo, and Aronne Armanini, "A Semi-Analytical Solution for the Dam-Break Problem Over a Movable Bed," *Proceedings of the 28th IAHR World Congress*, pp. 1-7, 1999. [Publisher Link]

[15] S. He et al., "An Improved Coupling Model for Water Flow, Sediment Transport and Bed Evolution," *Geoscientific Model Development Discussions*, vol. 7, pp. 2429-2457, 2014. [CrossRef] [Google Scholar] [Publisher Link]

[16] Guy Simpson, and Sébastien Castelltort, "Coupled Model of Surface Water Flow, Sediment Transport and Morphological Evolution," *Computers & Geosciences*, vol. 32, no. 10, pp. 1600-1614, 2006. [CrossRef] [Google Scholar] [Publisher Link]

[17] L.C. Van Rijn, "Sediment Transport, Part II: Suspended Load Transport," *Journal of Hydraulic Engineering*, vol. 110, no. 11, pp. 1613-1641, 1984. [CrossRef] [Google Scholar] [Publisher Link]